

# Water Resources Research



## RESEARCH ARTICLE

10.1029/2022WR033957

Daniel F. May and Bahareh Hassanpour contributed equally to this work.

#### **Key Points:**

- The synthesis-temperature-dependent hydrophobicity reduces the transport of fluorescent carbon nanoparticles through sand-packed columns
- A two-kinetic sites transport model describes the transport of fluorescent carbon nanoparticles in porous media
- Fluorescent carbon nanoparticles are not trapped in the meniscus under unsaturated conditions at the tested moisture contents

#### **Supporting Information:**

Supporting Information may be found in the online version of this article.

#### Correspondence to:

B. Hassanpour, Bahareh.Hassanpour@uwrf.edu

#### Citation:

May, D. F., Hassanpour, B., Sinclair, L., Steenhuis, T. S., & Cathles, L. M. (2023). Effect of hydrophobicity of fluorescent carbon nanoparticles on transport in porous media: Column experiments and modeling. *Water Resources Research*, 59, e2022WR033957. https://doi.org/10.1029/2022WR033957

Received 24 OCT 2022 Accepted 9 MAR 2023

#### **Author Contributions:**

Conceptualization: Daniel F. May, Bahareh Hassanpour, Laura Sinclair, Tammo S. Steenhuis, Lawrence M. Cathles

**Data curation:** Daniel F. May, Bahareh Hassanpour

Formal analysis: Daniel F. May, Bahareh Hassannour

Funding acquisition: Lawrence M. Cathles

**Investigation:** Daniel F. May, Bahareh Hassanpour

© 2023. The Authors.

This is an open access article under the terms of the Creative Commons Attribution License, which permits use, distribution and reproduction in any medium, provided the original work is properly cited.

# Effect of Hydrophobicity of Fluorescent Carbon Nanoparticles on Transport in Porous Media: Column Experiments and Modeling

Daniel F. May<sup>1,2,3</sup>, Bahareh Hassanpour<sup>4,5,6</sup>, Laura Sinclair<sup>7,8</sup>, Tammo S. Steenhuis<sup>2</sup>, and Lawrence M. Cathles<sup>1</sup>

<sup>1</sup>Department of Earth and Atmospheric Sciences, Cornell University, Ithaca, NY, USA, <sup>2</sup>Department of Biological and Environmental Engineering, Cornell University, Ithaca, NY, USA, <sup>3</sup>Now at Department of Geophysics, Stanford University, Stanford, CA, USA, <sup>4</sup>Department of Plant and Earth Science, University of Wisconsin-River Falls, River Falls, WI, USA, <sup>5</sup>Department of Agricultural Engineering Technology, University of Wisconsin-River Falls, River Falls, WI, USA, <sup>6</sup>Department of Biological Systems Engineering, University of Wisconsin-Madison, Madison, WI, USA, <sup>7</sup>Robert F. Smith School of Chemical and Biomolecular Engineering, Cornell University, Ithaca, NY, USA, <sup>8</sup>Now at CF Technologies, Hyde Park, MA, USA

Abstract Engineered carbon-based nanoparticles are increasingly used for environmental, industrial, and medical purposes. Thus, understanding their interaction with and transport through materials is important. We examine the impact of nanoparticle hydrophobicity and porous medium surface area on the transport of carbon nanoparticles through sand-packed columns under saturated and unsaturated conditions. The fluorescent carbon nanoparticles (FCNs) used in this study, synthesized from citric acid and ethanolamine, exhibit synthesis-temperature-dependent hydrophobicity. To quantify the impact of hydrophobicity on retention, we use FCNs synthesized at four temperatures: 190°C (FCN190), 210°C (FCN210), 230°C (FCN230), and 250°C (FCN250). Several observations are noted. First, the more hydrophobic particles (FCN230 and FCN250) attain lower outlet concentrations and mass recovery than more hydrophilic particles (FCN190 and FCN210). For instance, while 77% of the FCN190 was recovered after passing through a fine-sand-packed column, only 23% of the FCN250 was recovered. Second, sand surface area significantly impacts FCN recovery. A 17-fold increase in sand surface area yields a 30% decrease in the recovery of FCN210. Third, no significant difference in the mass recovery of the FCNs was observed between the unsaturated and saturated conditions, which is attributed to the small size of the FCNs relative to the water film thickness surrounding sand grains. Fourth, the particle transport model in HYDRUS-1D successfully simulated FCN transport, showing approximately a tenfold increase in the attachment coefficient for hydrophobic FCNs. In summary, through experiments and modeling, we show that hydrophobicity is a major factor impacting FCN transport.

# 1. Introduction

Engineered nanoparticles are increasingly used for industrial and environmental purposes (Ames et al., 2013; Galdames et al., 2020; Ko & Huh, 2019; Y. V. Li et al., 2014; Rudolph et al., 2020; Suzuki et al., 2018). An important class of engineering nanoparticles is carbon-based particles that exhibit unique physical and chemical properties that make them suitable for various applications (Hedayati et al., 2016). Carbon-based particles have applications in medicine and pharmaceuticals (He et al., 2013), energy sectors (Tan et al., 2012), wastewater treatment as an adsorbent (Tan et al., 2012), and industries such as optical materials (J. Wang et al., 2009). Fluorescent carbon nanoparticles (FCNs) have gained attention due to their optical properties, ease of synthesis, detection, and measurement, high stability and quantum yield, and biological and environmental compatibility (Krysmann et al., 2012; Qu & Sun, 2020; Y. Wang & Hu, 2014). Earlier versions of FCNs synthesized at 200°C from citric acid and ethanolamine have been used to describe flow patterns in experimental columns of glass beads (Subramanian et al., 2013) and calcium carbonate (Y. V. Li & Cathles, 2016; Y. V. Li et al., 2014). In the field, they have been used as an inert tracer to characterize flow in fractured quartzite in Altona, NY (Hawkins et al., 2017; Zhao, 2015) and long-term tracer tests in oil field carbonate rocks in Saudi Arabia (Kanj et al., 2011; Kosynkin & Alaskar, 2016). The small diffusion constant of these FCNs, less than one tenth that of anionic tracers such as Br or Cl, potentially allows them to detect preferential flow channels (Subramanian et al., 2013). The minimal attachment of these FCNs, synthesized at 200°C, has been attributed to the near-neutral surface charge (reported  $\zeta$ -potential  $\sim$ 0), small size, and hydrophilic

MAY ET AL. 1 of 12

Methodology: Daniel F. May, Bahareh Hassanpour, Laura Sinclair, Tammo S. Steenhuis, Lawrence M. Cathles Software: Bahareh Hassanpour Supervision: Tammo S. Steenhuis, Lawrence M. Cathles Visualization: Bahareh Hassanpour Writing – original draft: Daniel F. May, Bahareh Hassanpour Writing – review & editing: Daniel F. May, Bahareh Hassanpour, Laura Sinclair, Tammo S. Steenhuis, Lawrence M. Cathles

decoration (Y. V. Li et al., 2014; Subramanian et al., 2013). However, laboratory experiments showed that these FCNs are adsorbed on silica surfaces. Sinclair et al. (2020) noted that the attachment of these FCNs to quartz surfaces in quartz crystal microbalance experiments increased with their hydrophobicity and that the hydrophobicity of FCNs increased with their pyrolysis temperature due to carbonization and loss of hydrophilic functional groups. Sinclair et al. (2020) further showed that electrostatic forces are not responsible for attachment because the addition of electrolytes did not impact the attachment of particles to the quartz microbalance (Sinclair et al., 2020). With the widespread usage, production, and disposal of carbon-based nanoparticles and the expected increased use in future decades (J. Wang et al., 2008), investigating the factors that impact their transport in porous media is crucial (M. Wang et al., 2016). Temperature-sensitive hydrophobicity of FCNs allows investigation of the impact of hydrophobicity on the transport and retention of carbon-based nanoparticles in porous media.

Transport in porous media is affected by a mixture of physical and chemical properties of the transported particles and the media. These properties, which are often investigated by column tests, include grain size and surface area (Bradford et al., 2002; Morales et al., 2009) and the chemical characteristics of the media and transported particles (Johnson & Elimelech, 1995; Schijven et al., 2002; Torkzaban et al., 2007), including particle hydrophobicity (Wan & Wilson, 1994a). Under unsaturated moisture conditions, film straining of particles may occur, which depends on capillary forces and meniscus deformation and is, therefore, dependent on moisture content (film thickness) and particle sizes (Sang et al., 2013; Torkzaban et al., 2008; Wan & Tokunaga, 1997). Another important factor that impacts the transport of nanoparticles is the site blocking (occupation) of attachment sites (Johnson & Elimelech, 1995; Lu, Xu, et al., 2013; Mattison et al., 2011). This phenomenon depends on the particle abundance and the collector surface availability and controls particle penetration depth (Becker et al., 2015; Sun et al., 2015).

Models based on the convection—dispersion equation with first-order attachment are typically used to predict the fate of chemicals and particles in porous media (Goldberg et al., 2014; Morales et al., 2009; Tian et al., 2010). More complex transport models include terms that consider the chemical and physical heterogeneity in particle transport, including attachment (adsorption) and detachment (desorption), such as multisite kinetics and site blocking (Bradford et al., 2003; Goldberg et al., 2014; Schijven et al., 2002). In the current study, we investigate if a two-kinetic sites model can simulate the transport of FCNs in sand columns.

Column tests are an essential, long-established approach for investigating the transport of particles and chemicals through porous media and their interaction with grain surfaces. We report here the result of the column experiments and modeling of the transport of FCNs with varying hydrophobicity due to particle synthesis at different temperatures in porous media. The overarching objective of our study is to describe the impact of the hydrophobicity of FCNs on their transport. Our specific objectives are to (a) decipher the role of FCN hydrophobicity in their breakthrough in the sand columns, (b) investigate the impact of sand surface area on the retention of the FCNs, (c) explore the impact of unsaturated conditions on the transport of FCNs, and (d) model the transport of FCNs through a saturated porous medium and determine their transport parameters.

# 2. Material and Methods

# 2.1. FCN Synthesis and Characteristics

We used the same batch of FCNs produced and characterized by Sinclair et al. (2020). Briefly, FCNs were synthesized by continuously stirring citric acid monohydrate (Sigma Aldrich) with ethanolamine (EMD Millipore) with a 1:3 M ratio at 160°C for 30 min to produce a precursor, which was then pyrolyzed at 190°C, 210°C, 230°C, or 250°C for 2 hr (Sinclair et al., 2020). These FCN products were dialyzed for  $\sim$ 1 week to remove small molecule contaminants and finally lyophilized for >48 hr. The diameter of the particles synthesized at all temperatures was 13  $\pm$  8 nm, as measured by transmission electron microscopy (Sinclair et al., 2020). The fluorescence and hydrophobicity of the particles depend strongly on pyrolysis temperature. The fluorescent quantum yield increases from 11% at 190°C to a peak of 16% at 210°C and then declines to 10% at 230°C and 4% at 250°C. High-performance liquid chromatography and quartz crystal microbalance measurements showed particle hydrophobicity increases with synthesis temperature (Sinclair et al., 2020). Specifically, increasing the pyrolysis temperature beyond 210°C during FCN synthesis causes a decline in particle fluorescence and an increased particle hydrophobicity due to transformations of particle surface decoration (Sinclair et al., 2020).

MAY ET AL. 2 of 12

19447973, 2023, 3, Downloaded from https://agupubs.onlinelibrary.wiley.com/doi/10.1029/2022WR033957 by Un

Table 1           Properties of Sands Used for the Current Study Before Acid Washing and the Brunauer–Emmett–Teller (BET) Surface Area								
Sand type	Source	$d_{10}^{a}$ (mm)	$d_{50}^{a}$ (mm)	$d_{90}^{a}$ (mm)	Purity (% silica)	Porosity	BET surface area (m <sup>2</sup> /g)	
Fine	AGSCO Co.	0.075	0.11	0.135	99.5	0.45	$0.2592 \pm 0.0014$	
Medium	AGSCO Co.	0.23	0.28	0.49	99.5	0.43	$0.0148 \pm 0.0003$	
Coarse	Unimin	0.725	0.9	1.02	90	0.41	$0.0734 \pm 0.0005$	

<sup>&</sup>lt;sup>a</sup>According to manufacturers for untreated sand (see Figure S4 in Supporting Information S1 for particle size distribution).

#### 2.2. Breakthrough Experiments

For breakthrough experiments, we used fine, medium, and coarse sands (Table 1). According to the manufacturers, the sand purity was 99.5% for the fine and medium AGSCO sand and 90% for the coarse Unimin sand (Table 1), and impurities primarily included metal oxides. For instance, Unimin sand consisted of aluminum oxide (5.5%) and potassium oxide (2.5%). Therefore, the sands were treated with 10% nitric acid (Tian et al., 2012). We examined the surface composition of the sands after acid washing using a scanning electron microscope equipped with energy-dispersive spectroscopy (Text S1 in Supporting Information S1). Our analysis showed that the surface compositions of the clean sands were similar (>99% silica). The clean sands contained trace amounts of reactive minerals (aluminum, potassium, and iron <1%; Figures S1–S3 in Supporting Information S1). The porosity of the sand in the columns was measured using the water saturation method (Table 1).

The impact of FCN hydrophobicity was investigated by injecting FCNs synthesized at four different temperatures, described above, through fine sand (Table 2). To investigate the effect of surface area on FCN transport, FCN210 was injected through columns packed with different sand types. These particles (FCN210) were selected due to the higher quantum yield of these particles compared to the other FCNs (Sinclair et al., 2020). Similarly, FCN210 was used under unsaturated conditions to investigate the impact of moisture saturation on the transport of FCNs. A summary of the experimental treatments is shown in Table 2. Additional breakthrough experiments were conducted (data presented in Text S2 in Supporting Information S1). Separate bromide tracer experiments were carried out to determine porous media characteristics (Table 2).

The experiments were carried out in vertical, cylindrical columns (2 cm in diameter, 17 cm in length). The sand in the column was wet packed with deionized water. The bottom of the column consisted of a 20 µm nylon filter connected to a fraction collector (Figure 1). For saturated experiments, the top of the sand was kept 2 cm below the water level at the outlet to maintain saturated conditions in the column (Figure 1a). For unsaturated column experiments, we used the same column as the saturated experiments, but with 12 small holes on the side of the column to allow air exchange, a standard practice previously used when simulating unsaturated conditions in sand-packed columns (Lenhart & Saiers, 2002; Tian et al., 2012). The fraction collector was placed in a vacuum chamber connected to a bubble tower that controlled the suction at 40 cm (Figure 1b). The experiment began after a steady-state condition was achieved. After the experiment, sand moisture was measured by weighing the sand before and after oven-drying at 105°C for 24 hr. Both saturated and unsaturated tests were performed in at least duplicates (Table 2).

**Table 2**Summary of Experimental Treatment Presented in the Current Study

Experiments	Saturation	Media	Nanoparticles	No. of replicates
Hydrophobicity	Saturated	Fine sand	FCN190, FCN210, FCN230, and FCN250	3
Surface area	Saturated	Fine sand	FCN210	3
		Medium sand		2
		Coarse sand		2
Unsaturated	Unsaturated	Fine sand	FCN210	2
		Medium sand		2
Bromide	Saturated and unsaturated	Fine sand	-	2
		Medium sand		2

MAY ET AL. 3 of 12

19447973, 2023, 3, Downloaded from https://agupubs.onlinelibrary.wiley.com/doi/10.1029/2022WR033957 by University Of Wisconsin

Figure 1. Experimental setup for (a) saturated and (b) unsaturated column conditions.

After passing through two saturated soil pore volumes (PVs) of electrolyte solution (50 mM CaCl<sub>2</sub>), two PVs of the FCN solution (20 mg L<sup>-1</sup> FCN, 50 mM CaCl<sub>2</sub>, and 50 mg L<sup>-1</sup> KBr) were passed through the column. The brine concentration (50 mM CaCl<sub>2</sub>) was similar to that of Sinclair et al. (2020) in the FCN attachment to quartz microbalance investigation. The injection of FCN solution was followed by eight PVs of the electrolyte solution. The flow remained constant during the experiment at 1.25 mL min<sup>-1</sup> and was propelled with a syringe pump. During the experiments, samples were collected at  $\sim$ 3-min intervals using a fraction collector. The experiments were conducted under saturated and unsaturated conditions, as depicted in Figure 1.

# 2.3. Analysis

The Brunauer–Emmett–Teller (BET) surface area of sand was measured using the nitrogen sorption method using a Micromeritics ASAP2020 surface area analyzer (Hesse et al., 2020; Table 1). The concentration of FCNs was determined using an Agilent Cary Eclipse Fluorescence Spectrophotometer (Agilent Technologies, California, USA). The concentration of FCNs was measured in the influent and effluent samples at the excitation wavelength of 358 nm and peak emission wavelengths between 450 and 470 nm, and linear calibrations were constructed. A Dionex ICS-2000 Ion Chromatograph (Dionex, California, USA) was used to determine bromide concentrations. The statistical analysis was performed using JMP (Statistical Discovery<sup>TM</sup> from SAS). The Student's t test was used for the comparison between treatments.

# 2.4. Transport Model

To model the transport of FCNs, we used the particle transport model within HYDRUS-1D (Ver. 4.17.0140; Šimůnek Šejna, Saito, et al., 2013). HYDRUS-1D uses a finite element method to solve convective—dispersive equations numerically (Šimůnek Šejna, Saito, et al., 2013; Šimůnek & van Genuchten, 2008). This model simulates both uniform and nonequilibrium transport and solves inverse problems by fitting the best solution based on the lowest sum of squared residuals (SSQ; Šimůnek Šejna, Saito, et al., 2013).

Uniform transport used for conservative tracer (bromide) is described by the convection–dispersion equation:

$$\frac{\partial c}{\partial t} = D \frac{\partial^2 c}{\partial x^2} - v \frac{\partial c}{\partial x} \tag{1}$$

where c is the aqueous concentration [M L<sup>-3</sup>], t is time (T), D is the dispersion coefficient [L<sup>2</sup> T<sup>-1</sup>], v is the average pore water velocity [L T<sup>-1</sup>], and x is the spatial coordinate [L].

For the simulation of FCN transport in porous media, three models were tested and compared with the observed breakthrough curves (BTCs). The model that best simulated our experimental observations was a two-kinetic sites particle transport model which assumes due to physical and chemical reasons, the attachment on either

MAY ET AL. 4 of 12

**Table 3**Model Performance and Best Fit Parameters for Uniform Model (for Bromide) and Two-Site Kinetic Attachment/
Detachment Model (for FCNs) for the Fine Sand

Model	Model performance					Model best fit parameters					
Exp.	SSQ	$R^2$	$E_{ m f}$	MCE	CD	Disp.a (cm)	$s_{\text{max1}}$ (mg g <sup>-1</sup> )	$\begin{array}{c} k_{\rm a2} \\ (\rm min^{-1}) \end{array}$	$k_{\rm d2} \atop (\rm min^{-1})$	$k_{\rm al} \ ({ m min}^{-1})$	k <sub>d1</sub> (min <sup>-1</sup> )
Bromide	0.04	1.00	1.00	0.98	0.99	0.134	NA	NA	NA	NA	NA
FCN190	0.012	1.00	1.00	0.98	0.99	0.134 <sup>b</sup>	3.88 <sup>b,c</sup>	0.022	0.078	0.015	$0_{\mathbf{p}}$
FCN210	0.016	0.99	0.99	0.98	0.98	0.134 <sup>b</sup>	15.5 <sup>b,c</sup>	0.035	0.082	0.022	$0_{\mathbf{p}}$
FCN230	0.007	0.99	0.99	0.98	0.98	0.134 <sup>b</sup>	194.4 <sup>b,c</sup>	0.038	0.030	0.110	$0_{p}$
FCN250	0.015	1.00	0.99	0.98	0.99	0.134 <sup>b</sup>	327.4 <sup>b,c</sup>	0.018	0.049	0.079	0 <sub>p</sub>

*Note.* The  $R^2$  correlation coefficient, mean cumulative error (MCE), Nash-Sutcliffe model efficiency ( $E_f$ ), and coefficient of determination (CD) methods were used to quantify the quality of each of the model results.

<sup>a</sup>Longitudinal dispersivity (D/v, where D is the dispersion coefficient, and v is the velocity of water). <sup>b</sup>Fixed values. <sup>c</sup>Adapted from Sinclair et al. (2020).

site is kinetic (Šimůnek Šejna, Saito, et al., 2013). The one-site and the two-site kinetic models, which assume kinetic attachment at only one site, did not satisfactorily reproduce the observed BTCs (see Text S3 and Figure S6 in Supporting Information S1). Thus, we focused on the two-kinetic sites transport model (assuming kinetic attachment on two sites) which is described by

$$\frac{\partial c}{\partial t} + \frac{\rho}{\theta} \frac{\partial s_1}{\partial t} + \frac{\rho}{\theta} \frac{\partial s_2}{\partial t} = D \frac{\partial^2 c}{\partial x^2} - v \frac{\partial c}{\partial x}$$
 (2)

where subscripts 1 and 2 are the first and second kinetic attachment sites,  $\rho$  is the bulk density of the porous medium [M L<sup>-3</sup>],  $\theta$  is the volumetric moisture content [L<sup>3</sup> L<sup>-3</sup>], and  $s_1$  and  $s_2$  are the adsorbed concentrations on the first and second kinetic sorption sites [M M<sup>-1</sup>], respectively. Langmuirian dynamics govern the attachment of FCNs, as observed by Sinclair et al. (2020). Thus, at site 1, we assumed Langmuirian dynamics control the occupation, but detachment is not permitted (we take  $k_{d1} = 0$  in Equation 3). At site 2, kinetic attachment and detachment were allowed. Thus, the solid phase mass balance on sites 1 and 2 is given as

$$\rho \frac{\partial s_1}{\partial t} = \theta k_{\text{al}} \psi_1 c - \rho k_{\text{dl}} s_1 \tag{3}$$

$$\rho \frac{\partial s_2}{\partial t} = \theta k_{a2} c - \rho k_{d2} s_2 \tag{4}$$

where  $k_a$  and  $k_d$  [T<sup>-1</sup>] are the first-order attachment and detachment coefficients, respectively, and  $\psi_1$  is the dimensionless particle retention function which can be described by Langmuirian dynamics (Adamczyk et al., 1994):

$$\psi_1 = 1 - \frac{s_1}{s_{\text{max } 1}} \tag{5}$$

where  $s_{\text{max 1}}$  is the maximum solid phase concentration [M M<sup>-1</sup>]. To avoid fitting too many parameters, which may lead to nonunique solutions, we used the maximum solid phase concentrations measured using quartz microbalance by Sinclair et al. (2020). The maximum solid phase concentrations for FCN250, FCN230, FCN210, and FCN190 were 126, 75, 6, and 1.5 ng/cm<sup>2</sup>, respectively (Sinclair et al., 2020), and were used in the model after adjusting for the BET surface areas of the sands (Tables 1 and 3).

Simulations in HYDRUS-1D were performed for constant flux upper and lower flow boundary conditions, a first-type upper transport boundary condition with known concentrations, and a zero-concentration gradient as the lower transport boundary condition. The software executed the simulations for 101 nodes in the column profile and a minimum time step of 0.01 min.

MAY ET AL. 5 of 12

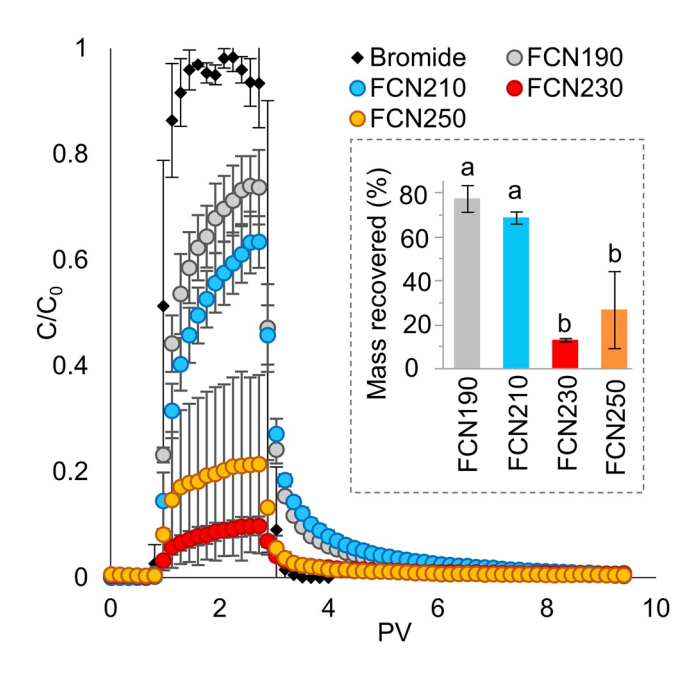


**Figure 2.** The breakthrough curves (normalized effluent concentrations  $[C/C_0]$  vs. pore volume [PV]) and the mass balances of fluorescent carbon nanoparticle (FCN) synthesized at different temperatures: FCN190, FCN210, FCN230, and FCN250 for the fine sand. Error bars indicate the standard deviations for the experimental replicates. Distinct letters above the mass recoveries indicate that the difference between the recovery of FCNs is significant (p < 0.05).

#### 2.5. Model Evaluation

Both graphical displays of the BTC and statistical assessments were used to evaluate how well the model fits the observed data. The BTCs were plotted as normalized effluent concentrations ( $C/C_0$ ) versus PVs after adjustment for the water trapped in the drainage tube ( $\sim$ 3 mL). For statistical assessments, we used (a) correlation coefficient ( $R^2$ ), (b) Nash–Sutcliffe model efficiency ( $E_{\rm f}$ ; Nash & Sutcliffe, 1970), (c) mean cumulative error (MCE; Perrin et al., 2001), and (d) coefficient of determination (CD; Loague & Green, 1991). The value of  $R^2$  ranges from 0 to 1, MCE and  $E_{\rm f}$  range from  $-\infty$  to 1, and CD ranges from 0 to  $\infty$ . A value of 1 represents a perfect fit for all these parameters.

The  $E_{\rm f}$  criterion is commonly used for evaluating model performance. If  $E_{\rm f}$  is less than zero, the simulated values are worse than the observed mean (Loague & Green, 1991). The  $E_{\rm f}$  is given as (Nash & Sutcliffe, 1970)

$$E_{\rm f} = 1 - \frac{\sum_{i=1}^{n} (C_{{\rm obs},i} - C_{{\rm sim},i})^2}{\sum_{i=1}^{n} \left(C_{{\rm obs},i} - \overline{C_{{\rm obs}}}\right)^2}$$
(6)

where  $\overline{C_{\text{obs}}}$  is the mean observed concentration during the experiment, and *i* denotes time. The MCE evaluates how well a model reproduces the concentrations over the entire experimental period, given as (Perrin et al., 2001)

$$MCE = 1 - \left| \sqrt{\frac{\sum_{i=1}^{n} C_{\text{sim},i}}{\sum_{i=1}^{n} C_{\text{obs},i}}} - \sqrt{\frac{\sum_{i=1}^{n} C_{\text{obs},i}}{\sum_{i=1}^{n} C_{\text{sim},i}}} \right|$$
(7)

where  $C_{\text{obs},i}$  is the observed concentration,  $C_{\text{sim},i}$  is the simulated concentration. The fourth criterion, CD, is a measure of the proportion of the total variances of observed data that are explained by the simulated values, expressed as (Loague & Green, 1991)

$$CD = \frac{\sum_{i=1}^{n} \left( C_{\text{obs},i} - \overline{C_{\text{obs}}} \right)^{2}}{\sum_{i=1}^{n} \left( C_{\text{sim},i} - \overline{C_{\text{obs}}} \right)^{2}}$$
(8)

# 3. Results and Discussion

# 3.1. Effect of Hydrophobicity on FCN Retention

To investigate the impact of hydrophobicity on the transport of particles, we analyzed saturated column experiments using three types of sands and four FCNs synthesized at different temperatures and bromide as a conservative tracer. A significant difference (p < 0.0001) was observed between the mass recovery of hydrophilic particles (FCN190 and FCN210) and hydrophobic particles (FCN230 and FCN250). The mass recovered in the effluent declined from 77% for FCN190% to 23% for FCN250 (Figure 2). These observations were in line with the greater hydrophobicity of FCNs pyrolyzed at higher temperatures (Sinclair et al., 2020). The hydrophobicity of organic nanoparticles is known to be an important factor in their interactions with mineral surfaces (Gessner et al., 2000; Lundqvist et al., 2008).

The breakthrough of FCNs and bromide occurred at the same time. However, while bromide concentrations reached  $C/C_0 \approx 1$  at about PV  $\approx 1.5$ , the  $C/C_0$  for FCN190, FCN210, FCN230, and FCN250 gradually reached a plateau at 0.7, 0.6, 0.1, and 0.2, respectively (Figure 2). While bromide concentrations decreased rapidly to zero at PV = 3.5, FCNs exhibited long tails (Figure 2). This asymmetrical breakthrough with long tails points to a nonequilibrium transport, in which the attachment is rate limited (van Genuchtern, 1981), and was previously observed for nanoparticles in porous media (Hu et al., 2017; Johnson & Elimelech, 1995; Kasel et al., 2012; Lu, Xu, et al., 2013; Lu, Yang, et al., 2013; Mattison et al., 2011).

MAY ET AL. 6 of 12

on Wiley Online Library for rules of use; OA articles are governed by the applicable Creat

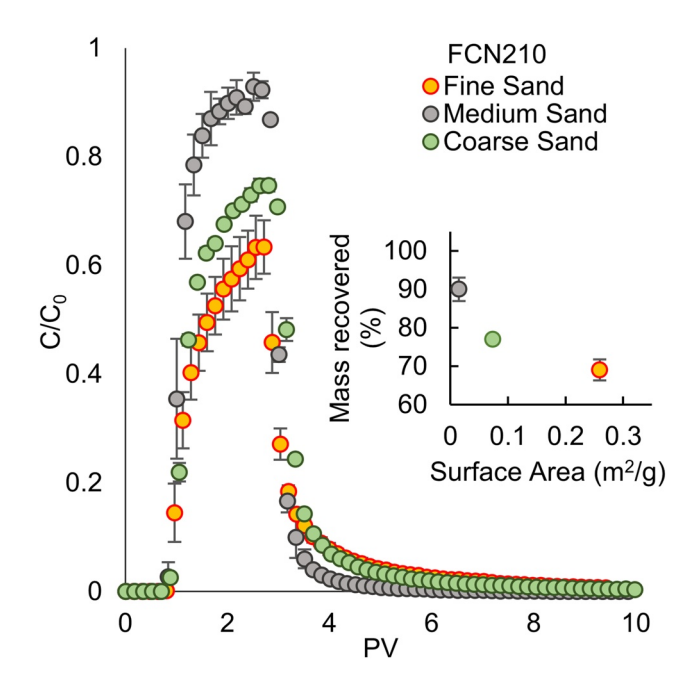


**Figure 3.** The breakthrough curves (normalized effluent concentrations  $[C/C_0]$  vs. pore volume [PV]) of FCN210 for medium, fine, and coarse sands and the relationship between sand surface area and the recovery of FCN210. Error bars indicate the standard deviations for the experimental replicates for the fine sand and duplicates for the medium and coarse sand.

#### 3.2. Effect of Grain Surface Area on FCN Retention

To illustrate the impact of sand surface area on the recovery of FCNs, we chose to focus on the transport of FCN210 in saturated sands due to its higher quantum yield and hydrophilicity compared to the other FCNs (Sinclair et al., 2020). Figure 3 presents the BTC and the mass balance of FCN210 for sands with different surface areas. The  $C/C_0$  of FCN210 for the medium sand reached  $\sim 0.92$  at PV = 2.5, while for the fine sand and coarse sand, the  $C/C_0$  reached 0.63 and 0.74, respectively (Figure 3). The recovery of the FCN210 through fine sand (69%) was the lowest among the sands (Figure 3). But notably, the recovery of FCN210 through the medium sand was greater than that through the coarse sand (Figure 3; p < 0.002). This lower recovery through the coarse sand in comparison to that of medium sand is due to the larger number of collector sites, as evidenced by the larger BET surface area (Table 1), which leads to increased retention of FCNs (Figure 3; Mekonen et al., 2014). This larger surface area of the coarse sand compared to the medium sand is attributed to its greater surface roughness, leading to increased particle attachment sites (Morales et al., 2009).

Another factor mentioned in the literature affecting recovery is straining, defined as the trapping of particles in small pore throats and is related to the sizes of particles and medium grains (Crist et al., 2005; Lu, Xu, et al., 2013). Straining occurs when the particle to grain diameter ratio exceeds a certain threshold (Wan & Tokunaga, 1997), for instance, 0.008 (Xu et al., 2006) or 0.0017 (Bradford et al., 2002). However, for the FCNs and sands used in this study, this ratio is 1-2 orders of magnitude smaller than these thresholds  $(1.4 \times 10^{-5})$  for coarse sand and  $1.3 \times 10^{-4}$  for fine

sand). Therefore, straining was not likely to contribute to FCN retention in our experiments. Similarly, Y. Li et al. (2008) showed that straining did not occur for fullerene nanoparticles in quartz sand with a diameter ratio of 0.0002.

### 3.3. Effect of Unsaturated Conditions

To examine the role of the air—water—solid interface on the retention of FCNs, we conducted unsaturated experiments. Figures 4a and 4b show the BTCs of the FCN210 and bromide under unsaturated conditions through the fine and medium sand columns. The arrival of FCNs and bromide tracer occurred earlier under unsaturated conditions than under saturated conditions (Figures 2–4). This early arrival is especially noticeable for the

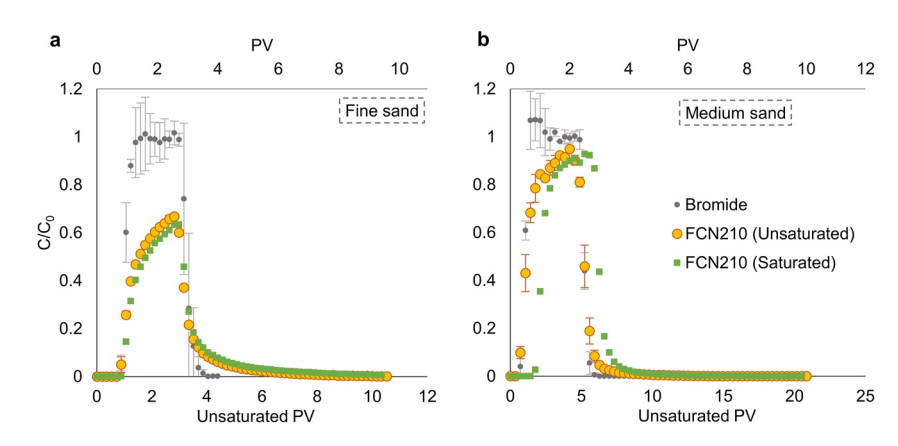


**Figure 4.** Fluorescent carbon nanoparticle (FCN) breakthrough curves (normalized effluent concentrations  $[C/C_0]$  vs. unsaturated pore volume [unsaturated PV] and total pore volume [PV]) under unsaturated conditions for the (a) fine and (b) medium sands for bromide and FCN210. Error bars indicate the standard deviations for the experimental duplicates.

MAY ET AL. 7 of 12

medium sand with a lower saturation level (48% in medium sand vs. 90% in fine sand). This difference in saturation level is due to the greater water-holding capacity of the finer sands under the same capillary tension (set at 40 cm). However, the shape of the BTCs, the recovery, and, thus, the mass balances of the FCNs were similar under unsaturated and saturated conditions (p > 0.05; Figure 4). Similar results were observed for FCN190 in fine and medium sand (Figure S5 in Supporting Information S1).

When air and water are both present in the pore space, colloidal-size particles can be strained in water film and air—water—solid interfaces (Gao et al., 2008; Wan & Tokunaga, 1997; Wan & Wilson, 1994b). Wan and Tokunaga (1997) suggest that colloids are trapped in thin water films as the saturation drops to a point where pendular rings become disconnected, or the diameter of the particles exceeds the thickness of the film, after which capillary forces retain the particles on the grain surface. These forces are related to the deformation of the water film (Gao et al., 2008). Given that we did not observe a difference in the retention of particles, our results indicate that film straining did not contribute to the retention of FCNs in porous media (Gao et al., 2008; Zevi et al., 2006). This can be explained by the small diameter of the FCNs and the relatively high column saturation in which films stayed connected. Similarly, in another study with column saturations greater than 16%, no additional retention of carbon nanotubes with diameters of 20–30 nm and lengths of 0.5–2  $\mu$ m was observed under unsaturated conditions (Mekonen et al., 2014).

## 3.4. Transport Modeling

The FCN concentrations in the effluent of the fine sand column for the four saturated hydrophobicity experiments (Table 1) were used to investigate the effect of hydrophobicity on the parameters of the two-kinetic sites particle transport model (Equations 2–5). The dispersivity and the flow velocity in the columns were obtained by fitting the bromide tracer experiments concentrations against the convective dispersive equation (Equation 1).

As expected, the convection–dispersion equation fits the bromide BTC concentrations well, evident from the simulated and observed BTCs (Figure 5a) and the statistical assessment of the model (Table 3). The  $R^2$ ,  $E_f$ , MCE, and CD for simulated BTC of bromide varied between 0.96 and 1 (Table 2). The best fit dispersivity value for the fine sand, 0.134 cm, is within the values reported previously in small experimental columns and sandy media (Table 2; Lal & Shukla, 2005; Perfect et al., 2002).

The two-kinetic sites particle transport model successfully simulated the BTC of all four FCNs in fine sand, and  $R^2$ ,  $E_{\rm P}$  MCE, and CD values varied between 0.94 and 1 (Table 2). This two-kinetic sites particle transport model also fits the coarse and medium sand BTCs well (Text S4 and Figure S7 in Supporting Information S1). As summarized in Table 3, the best fit model values of  $k_{\rm a2}$  for FCNs (Equations 2–5) obtained with the HYDRUS 1D model varied between 0.02 and 0.04 min<sup>-1</sup>, and the best fit values of  $k_{\rm d2}$  were 0.03–0.08 min<sup>-1</sup>. The  $k_{\rm a1}$  values, however, were nearly an order of magnitude greater for the more hydrophobic FCNs than those for the more hydropholic FCNs. The best fit  $k_{\rm a1}$  values were 0.01–0.02 min<sup>-1</sup> for FCN190 and FCN210, independent of sand type (Table 3 and Table S2 in Supporting Information S1). These values increased to 0.08 and 0.11 min<sup>-1</sup> for the FCN250 and FCN230 (Table 2). Note that these values are independent of the maximum solid phase concentration,  $s_{\rm max\,1}$ , since the applied mass of FCNs (~1.4 mg) is many times smaller than that can be absorbed in the column, making the last term in Equation 5 nearly zero. Figure S8 in Supporting Information S1 shows that 2 orders of magnitude change in  $s_{\rm max\,1}$  leads to small changes (<7%) in estimated  $C/C_0$  values.

The best fit values for  $k_{\rm al}$  were within those observed for carbon nanotubes in sand (Kasel et al., 2012; Zhang et al., 2019) and goethite-coated sand (Zhang et al., 2016), despite the differences in the composition of carbon-based particles, the media, flow rate, and electrolyte solution. Our observations agree with those of Sinclair et al. (2020), which showed that the attachment to quartz surfaces of FCN230 and FCN250 was greater than for FCN190 and FCN210. This is interpreted as the result of the transformation of their surface chemistry at synthesis temperatures >210°C leading to an increased hydrophobicity. Thus, the greater values of the attachment coefficient on site 1, when the FCN hydrophobicity increases, indicated that site 1 primarily represents hydrophobic interactions. We assume that the hydrophobic interactions at this site are irreversible (G. Li et al., 2002) and take  $k_{\rm dl}$  to be zero.

Our modeling shows that interactions on two kinetic sites were essential to successfully simulate these nanoparticles' transport. With particle detachment not allowed, site 1 acts as a sink where interactions are primarily hydrophobic and irreversible. Hydrophobic associations between the adsorbate and mineral surface play an essential role in organo-mineral interactions (Coward et al., 2019). On site 2, however, there is a high exchange

MAY ET AL. 8 of 12

19447973, 2023, 3, Downloaded from https://agupubs.onlinelibrary.wiley.com/doi/10.1029/2022WR033957 by University Of Wisconsin, Wiley Online Library on [05/06/2023]. See the Terms and Conditions (https://onlinelibrary.wiley

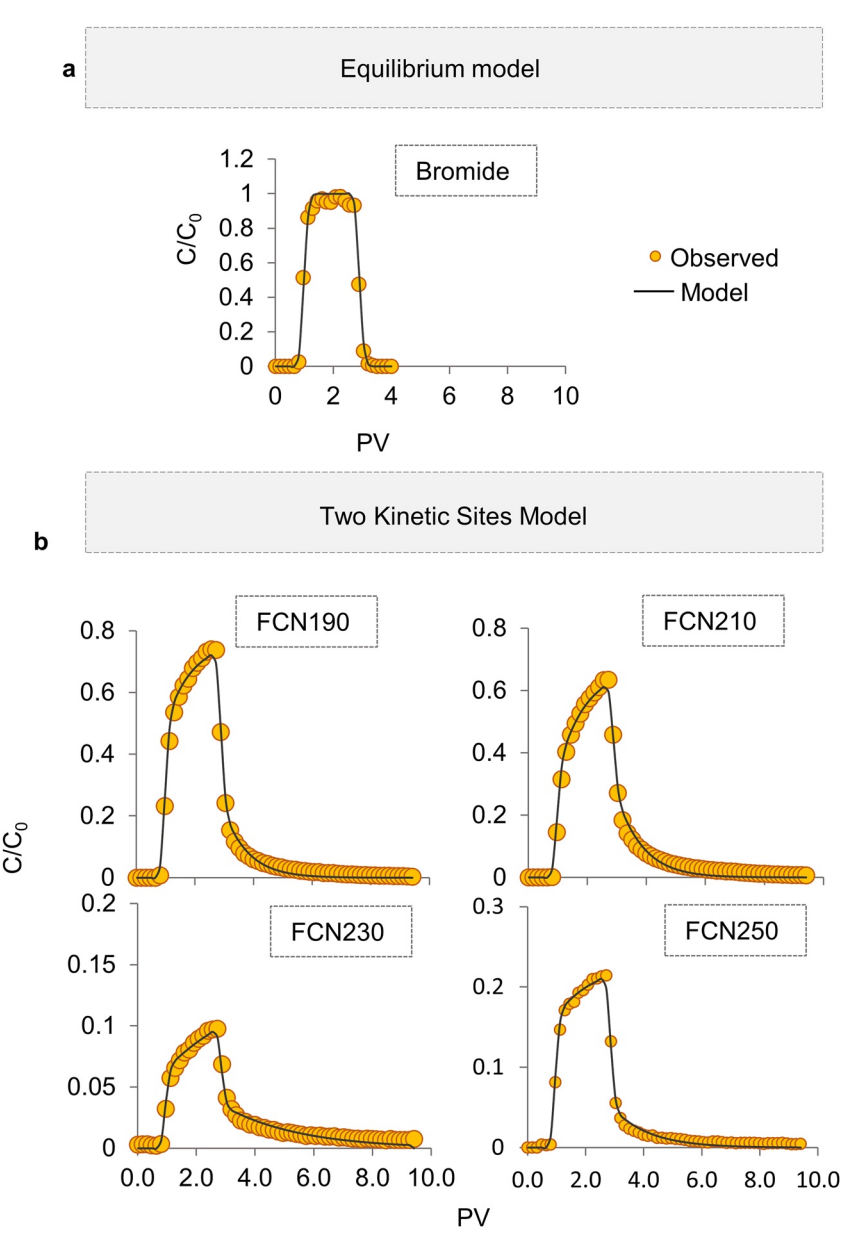


Figure 5. Measured and modeled breakthrough curves for the fine sand under saturated conditions. The data points are the average concentrations of three replicates.

rate of attachment and detachment, which captures the asymmetry of the BTCs (Figure S9 in Supporting Information S1). The transport model does not capture the underlying reason behind these interactions which requires molecular scale investigations. However, an explanation could be the creation of a "kinetic zone" due to the hierarchical attachment of FCNs on sand surfaces due to the heterogeneity of the functional groups on their surfaces (Kleber et al., 2007). In this view, FCNs attached on site 1 create reversible attachment sites (site 2) for other FCNs leading to a hierarchical assembly (Coward et al., 2019; Kleber et al., 2007). Further, the heterogeneity of the sand surface and FCNs could create the second attachment site. Thus, a combination of hydrophobic and electrostatic interactions may have played a role, although, using quartz microbalance, Sinclair et al. (2020) reported a minimal role of electrostatic interactions because varying the ionic strength of the solution did not affect the attachment. Nevertheless, we showed that the two-kinetic sites model gives a good description of the BTCs and the asymmetry of the BTC. The experiments, modeling, and conceptualization presented in the current study could have broad applications in understanding the transport of carbon-based nanomaterials and the impact of hydrophobicity on their transport in porous media.

MAY ET AL. 9 of 12

19447973, 2023, 3, Downloaded from https://agupubs

doi/10.1029/2022WR033957 by University Of Wisconsin, Wiley Online Library on [05/06/2023]. See

# 4. Conclusions

Due to their hydrophilicity (if synthesized at low temperature) and high quantum yield (which makes the measurement of particle concentration easy), FCNs have been successful in characterizing subsurface water transport. This study examined the role of the hydrophobicity, sand grain surface area, and saturation of the porous media on the transport of FCNs using column experiments and pulse application of FCNs. Hydrophobicity and surface area of the porous media impacted the transport of FCNs. Saturation levels, however, did not have an impact on FCN retention. Increased hydrophobicity led to a 60% decrease in the FCN recovery, while increased surface area led to a 30% decrease. A particle transport model with two-kinetic attachment/detachment sites in HYDRUS-1D software package successfully simulated the transport of FCNs. Kinetic occupation with no detachment on one site, site 1, controls the hydrophobic retention observed, while reversible retention on a second site controls the shape of the BTCs and captures the asymmetry of the BTCs. On site 1, an order of magnitude difference between the attachment coefficients of the hydrophobic and hydrophilic FCNs to sand was determined. Further molecular work is needed to describe the physiochemical reasons for irreversible and reversible kinetic attachment on these two sites. Site blocking and straining, however, had minimal impact. A broader application of this study is the illustration of how the variable hydrophobicity of the FCNs described and tested here can be used to better understand the role of hydrophobicity in the transport of carbon-based nanoparticles and organic nanoparticle contaminants in porous media.

#### **Conflict of Interest**

The authors declare no conflicts of interest relevant to this study.

# **Data Availability Statement**

Experimental and modeling data used in the manuscript and supplementary material are available for download (May et al., 2023) at the open repository Zenodo via https://doi.org/10.5281/zenodo.7643954 (license: Creative Commons Attribution 4.0 International, no access restrictions). This data set includes the results column experiments for both unsaturated and saturated conditions; the breakthrough curve modeling results generated using the three models discussed in this study for comparison with the saturated column experiments; model output files for the two-kinetic sites modeling; and the data from the characterization of the sand surfaces using scanning electron microscope. HYDRUS-1D version 4.17.0140 (Šimůnek, Šejna, & van Genuchten, 2013) was used for modeling the transport of FCNs in porous media and is available at https://www.pc-progress.com/en/Default.aspx.

### Acknowledgments

The authors would like to thank Dr Ludmilla Aristilde and Dr Jefferson Tester for the use of fluorescence equipment. BET surface area facilities were provided by Dr Uli Wiesner, Cornell University, and we are especially grateful for help from Paxton Thedford, This work made use of an SEM-EDX acquired through NSF-MRI-2116671. We also would like to thank Dr Kevin Thaisen and Dr Samuel Alvarado for their assistance with SEM-EDX analysis. The authors thank Dr Joseph Brown and Dr Adam Hawkins for the insightful discussions. Finally, special thanks to Fardad Riazi for assisting in carrying out the experiments. Support for Bahareh Hassanpour during this study was provided by Wisconsin Dairy Innovation Hub. Gifts from the Pall Corporation and the Norwegian Improved Oil Recovery project are gratefully acknowledged.

# References

- Adamczyk, Z., Siwek, B., Zembala, M., & Belouschek, P. (1994). Kinetics of localized adsorption of colloid particles. Advances in Colloid and Interface Science, 48, 151–280. https://doi.org/10.1016/0001-8686(94)80008-1
- Ames, M., Li, K., & Horne, R. N. (2013). The utility of threshold reactive tracers for characterizing temperature distributions in geothermal reservoirs. Paper presented at Proceedings of the Thirty-Eighth Workshop on Geothermal Reservoir Engineering SGP-TR-198.
- Becker, M. D., Wang, Y., Pennell, K. D., & Abriola, L. M. (2015). A multi-constituent site blocking model for nanoparticle and stabilizing agent transport in porous media. *Environmental Science: Nano*, 2(2), 155–166. https://doi.org/10.1039/C4EN00176A
- Bradford, S. A., Simunek, J., Bettahar, M., van Genuchten, M. T., & Yates, S. R. (2003). Modeling colloid attachment, straining, and exclusion in saturated porous media. *Environmental Science & Technology*, 37(10), 2242–2250. https://doi.org/10.1021/es025899u
- Bradford, S. A., Yates, S. R., Bettahar, M., & Simunek, J. (2002). Physical factors affecting the transport and fate of colloids in saturated porous media. Water Resources Research, 38(12), 1327. https://doi.org/10.1029/2002WR001340
- Coward, E. K., Ohno, T., & Sparks, D. L. (2019). Direct evidence for temporal molecular fractionation of dissolved organic matter at the iron oxyhydroxide interface. Environmental Science & Technology, 53(2), 642–650. https://doi.org/10.1021/acs.est.8b04687
- Crist, J. T., Zevi, Y., McCarthy, J. F., Throop, J. A., & Steenhuis, T. S. (2005). Transport and retention mechanisms of colloids in partially saturated porous media. *Vadose Zone Journal*, 4(1), 184–195. https://doi.org/10.2113/4.1.184
- Galdames, A., Ruiz-Rubio, L., Orueta, M., Sanchez-Arzalluz, M., & Vilas-Vilela, J. L. (2020). Zero-valent iron nanoparticles for soil and ground-water remediation. *International Journal of Environmental Research and Public Health*, 17(16), 5817. https://doi.org/10.3390/ijerph17165817
   Gao, B., Steenhuis, T. S., Zevi, Y., Morales, V. L., Nieber, J. L., Richards, B. K., et al. (2008). Capillary retention of colloids in unsaturated porous media. *Water Resources Research*, 44, W04504. https://doi.org/10.1029/2006WR005332
- Gessner, A., Waicz, R., Lieske, A., Paulke, B. R., Mader, K., & Muller, R. (2000). Nanoparticles with decreasing surface hydrophobicities: Influence on plasma protein adsorption. *International Journal of Pharmaceutics*, 196(2), 245–249. https://doi.org/10.1016/s0378-5173(99)00432-9 Goldberg, E., Scheringer, M., Bucheli, T. D., & Hungerbühler, K. (2014). Critical assessment of models for transport of engineered nanoparticles

in saturated porous media. Environmental Science & Technology, 48(21), 12732–12741. https://doi.org/10.1021/es502044k

MAY ET AL. 10 of 12

- Hawkins, A. J., Fox, D. B., Becker, M. W., & Tester, J. W. (2017). Measurement and simulation of heat exchange in fractured bedrock using inert and thermally degrading tracers. Water Resources Research, 53, 1210–1230. https://doi.org/10.1002/2016WR019617
- He, H., Pham-Huy, L. A., Dramou, P., Xiao, D., Zuo, P., & Pham-Huy, C. (2013). Carbon nanotubes: Applications in pharmacy and medicine. BioMed Research International, 2013, 578290. https://doi.org/10.1155/2013/578290
- Hedayati, M., Sharma, P., Katyal, D., & Fagerlund, F. (2016). Transport and retention of carbon-based engineered and natural nanoparticles through saturated porous media. *Journal of Nanoparticle Research*, 18(3), 57. https://doi.org/10.1007/s11051-016-3365-6
- Hesse, S. A., Fritz, K. E., Beaucage, P. A., Thedford, R. P., Yu, F., DiSalvo, F. J., et al. (2020). Materials combining asymmetric pore structures with well-defined mesoporosity for energy storage and conversion. ACS Nano, 14(12), 16897–16906. https://doi.org/10.1021/acsnano.0C05903
- Hu, Z., Zhao, J., Gao, H., Nourafkan, E., & Wen, D. (2017). Transport and deposition of carbon nanoparticles in saturated porous media. *Energies*, 10(8), 1151. https://doi.org/10.3390/en10081151
- Johnson, P. R., & Elimelech, M. (1995). Dynamics of colloid deposition in porous media: Blocking based on random sequential adsorption. Langmuir, 11(3), 801–812. https://doi.org/10.1021/la00003a023
- Kanj, M. Y., Rashid, M. H., & Giannelis, E. P. (2011). Industry first field trial of reservoir nanoagents. SPE.
- Kasel, D., Bradford, S. A., Šimůnek, J., Heggen, M., Vereecken, H., & Klumpp, E. (2012). Transport and retention of multi-walled carbon nanotubes in saturated porous media: Effects of input concentration and grain size. Water Research, 47(2), 933–944. https://doi.org/10.1016/j. watres.2012.11.019
- Kleber, M., Sollins, P., & Sutton, R. (2007). A conceptual model of organo-mineral interactions in soils: Self-assembly of organic molecular fragments into zonal structures on mineral surfaces. *Biogeochemistry*, 85(1), 9–24. https://doi.org/10.1007/s10533-007-9103-5
- Ko, S., & Huh, C. (2019). Use of nanoparticles for oil production applications. *Journal of Petroleum Science and Engineering*, 172, 97–114. https://doi.org/10.1016/j.petrol.2018.09.051
- Kosynkin, D., & Alaskar, M. (2016). Oil industry first interwell trial of reservoir nanoagent tracers. In T. George, A. K. Dutta, & M. S. Islam (Eds.), SPE Annual Technical Conference and Exhibition (p. 94671D). SPE.
- Krysmann, M. J., Kelarakis, A., Dallas, P., & Giannelis, E. P. (2012). Formation mechanism of carbogenic nanoparticles with dual photoluminescence emission. *Journal of the American Chemical Society*, 134(2), 747–750. https://doi.org/10.1021/ja204661r
- Lal, R., & Shukla, M. (2005). Principles of soil physics.
- Lenhart, J. J., & Saiers, J. E. (2002). Transport of silica colloids through unsaturated porous media: Experimental results and model comparisons. Environmental Science & Technology, 36(4), 769–777. https://doi.org/10.1021/es0109949
- Li, G., Doblhofer, K., & Fuhrhop, J.-H. (2002). Irreversible adsorption of cellobiose, ascorbic acid, and tyrosine to hydrophobic surfaces in water and their separation by molecular stirring. Angewandte Chemie International Edition, 41(15), 2730–2734. https://doi. org/10.1002/1521-3773(20020802)41:15<2730::AID-ANIE2730>3.0.CO:2-7
- Li, Y., Wang, Y., Pennell, K. D., & Briola, L. M. A. (2008). Investigation of the transport and deposition of fullerene (C60) nanoparticles in quartz sands under varying flow conditions. *Environmental Science & Technology*, 42(19), 7174–7180. https://doi.org/10.1021/es801305Y
- Li, Y. V., & Cathles, L. M. (2016). The surface interactions of a near-neutral carbon nanoparticle tracer with calcite. *Journal of Nanoparticle Research*, 18(3), 71. https://doi.org/10.1007/s11051-016-3383-4
- Li, Y. V., Cathles, L. M., & Archer, L. A. (2014). Nanoparticle tracers in calcium carbonate porous media. *Journal of Nanoparticle Research*, 16(8), 2541. https://doi.org/10.1007/s11051-014-2541-9
- Loague, K., & Green, R. E. (1991). Statistical and graphical methods for evaluating solute transport models: Overview and application. *Journal of Contaminant Hydrology*, 7(1–2), 51–73. https://doi.org/10.1016/0169-7722(91)90038-3
- Lu, Y., Xu, X., Yang, K., & Lin, D. (2013). The effects of surfactants and solution chemistry on the transport of multiwalled carbon nanotubes in quartz sand-packed columns. *Environmental Pollution*, 182, 269–277. https://doi.org/10.1016/j.envpol.2013.07.034
- Lu, Y., Yang, K., & Lin, D. (2013). Transport of surfactant-facilitated multiwalled carbon nanotube suspensions in soil columns. *Environmental Pollution*, 192, 36–43. https://doi.org/10.1016/j.envpol.2014.05.008
- Lundqvist, M., Stigler, J., Elia, G., Lynch, I., Cedervall, T., & Dawson, K. A. (2008). Nanoparticle size and surface properties determine the protein corona with possible implications for biological impacts. Proceedings of the National Academy of Sciences of the United States of America, 105(38), 14265–14270. https://doi.org/10.1073/PNAS.0805135105
- Mattison, N. T., O'Carroll, D. M., Kerry Rowe, R., & Petersen, E. J. (2011). Impact of porous media grain size on the transport of multi-walled carbon nanotubes. *Environmental Science & Technology*, 45(22), 9765–9775. https://doi.org/10.1021/es2017076
- May, D. F., Hassanpour, B., Sinclair, L., Steenhuis, T. S., & Cathles, L. M. (2023). Effect of hydrophobicity of fluorescent carbon nanoparticles on transport in porous media: Column experiment data and modeling (version 1) [Dataset]. Zenodo. https://doi.org/10.5281/zenodo.7643954
- Mekonen, A., Sharma, P., & Fagerlund, F. (2014). Transport and mobilization of multiwall carbon nanotubes in quartz sand under varying saturation. *Environmental Earth Sciences*, 71(8), 3751–3760. https://doi.org/10.1007/s12665-013-2769-1
- Morales, V. L., Gao, B., & Steenhuis, T. S. (2009). Grain surface-roughness effects on colloidal retention in the Vadose zone. Vadose Zone Journal, 8(1), 11–20. https://doi.org/10.2136/vzi2007.0171
- Nash, J. E., & Sutcliffe, J. v. (1970). River flow forecasting through conceptual models Part I—A discussion of principles. *Journal of Hydrology (Amsterdam)*, 10(3), 282–290. https://doi.org/10.1016/0022-1694(70)90255-6
- Perfect, E., Sukop, M. C., & Haszler, G. R. (2002). Prediction of dispersivity for undisturbed soil columns from water retention parameters. Soil Science Society of America Journal, 66(3), 696–701. https://doi.org/10.2136/sssaj2002.0696
- Perrin, C., Michel, C., & Andréassian, V. (2001). Does a large number of parameters enhance model performance? Comparative assessment of common catchment model structures on 429 catchments. *Journal of Hydrology (Amsterdam)*, 242(3–4), 275–301. https://doi.org/10.1016/S0022-1694(00)00393-0
- Qu, D., & Sun, Z. (2020). The formation mechanism and fluorophores of carbon dots synthesized via a bottom-up route. *Materials Chemistry Frontiers*, 4(2), 400–420. https://doi.org/10.1039/c9qm00552h
- Rudolph, B., Berson, J., Held, S., Nitschke, F., Wenzel, F., Kohl, T., & Schimmel, T. (2020). Development of thermo-reporting nanoparticles for accurate sensing of geothermal reservoir conditions. *Scientific Reports*, 10, 11422. https://doi.org/10.1038/s41598-020-68122-y
- Sang, W., Morales, V. L., Zhang, W., Stoof, C. R., Gao, B., Schatz, A. L., et al. (2013). Quantification of colloid retention and Release by straining and energy minima in variably saturated porous media. *Environmental Science & Technology*, 47, 130724151622003. https://doi.org/10.1021/ es400288c
- Schijven, J. F., Hassanizadeh, S. M., & de Bruin, R. H. A. M. (2002). Two-site kinetic modeling of bacteriophages transport through columns of saturated dune sand. *Journal of Contaminant Hydrology*, 57(3–4), 259–279. https://doi.org/10.1016/S0169-7722(01)00215-7
- Šimůnek, J., Šejna, M., Saito, H., Sakai, M., & van Genuchten, M. T. (2013). The HYDRUS-1D software package for simulating the one-dimensional movement of water, heat, and multiple solutes in variably-saturated media. Version 4.17.

MAY ET AL. 11 of 12

- Šimůnek, J., Šejna, M., & van Genuchten, M. T. (2013). HYDRUS-1D, version 4.17.0140. Code for simulating the one-dimensional movement if water, heat, and multiple solutes in variability saturated porous media [Software]. Retrieved from https://www.pc-progress.com/en/Default.aspx?hydrus
- Šimůnek, J., & van Genuchten, M. T. (2008). Modeling nonequilibrium flow and transport processes using HYDRUS. *Vadose Zone Journal*, 7(2), 782–797. https://doi.org/10.2136/vzj2007.0074
- Sinclair, L., Brown, J., Salim, M. G., May, D., Guilvaiee, B., Hawkins, A., & Cathles, L. (2020). Optimization of fluorescence and surface adsorption of citric acid/ethanolamine carbon nanoparticles for subsurface tracers. Carbon, 169, 395–402. https://doi.org/10.1016/j. carbon.2020.07.024
- Subramanian, S. K., Li, Y., & Cathles, L. M. (2013). Assessing preferential flow by simultaneously injecting nanoparticle and chemical tracers. Water Resources Research, 49, 29–42. https://doi.org/10.1029/2012WR012148
- Sun, Y., Gao, B., Bradford, S. A., Wu, L., Chen, H., Shi, X., & Wu, J. (2015). Transport, retention, and size perturbation of graphene oxide in saturated porous media: Effects of input concentration and grain size. Water Research, 68, 24–33. https://doi.org/10.1016/j.watres.2014.09.025
- Suzuki, A., Cui, J., Zhang, Y., Mohamed, A. R., Zein, S. H. S., & Tan, S. H. (2018). Nano-/microparticle tracers for evaluating structures in fractured porous media. *Paper presented at Stanford Geothermal Workshop SGP-TR-213*.
- Tan, K. H., Ong, Y. T., Mohamed, A. R., Zein, S. H. S., & Tan, S. H. (2012). Energy and environmental applications of carbon nanotubes. Environmental Chemistry Letters, 10(3), 265–273. https://doi.org/10.1007/s10311-012-0356-4
- Tian, Y., Gao, B., Morales, V. L., Wang, Y., & Wu, L. (2012). Effect of surface modification on single-walled carbon nanotube retention and transport in saturated and unsaturated porous media. *Journal of Hazardous Materials*, 239(240), 333–339. https://doi.org/10.1016/j. jhazmat.2012.09.003
- Tian, Y., Gao, B., Silvera-Batista, C., & Ziegler, K. J. (2010). Transport of engineered nanoparticles in saturated porous media. *Journal of Nanoparticle Research*, 12(7), 2371–2380. https://doi.org/10.1007/s11051-010-9912-7
- Torkzaban, S., Bradford, S. A., van Genuchten, M. T., & Walker, S. L. (2008). Colloid transport in unsaturated porous media: The role of water content and ionic strength on particle straining. *Journal of Contaminant Hydrology*, 96(1–4), 113–127. https://doi.org/10.1016/j.iconhyd.2007.10.006
- Torkzaban, S., Bradford, S. A., & Walker, S. L. (2007). Resolving the coupled effects of hydrodynamics and DLVO forces on colloid attachment in porous media. *Langmuir*, 23(19), 9652–9660. https://doi.org/10.1021/la700995e
- van Genuchtern, M. (1981). Non-equilibrium transport parameters from miscible displacement experiments.
- Wan, J., & Tokunaga, T. K. (1997). Film straining of colloids in unsaturated porous media: Conceptual model and experimental testing. Environmental Science & Technology, 31(8), 2413–2420. https://doi.org/10.1021/es970017q
- Wan, J., & Wilson, J. L. (1994a). Colloid transport in unsaturated porous media. Water Resources Research, 30(4), 857–864. https://doi.org/10.1029/93WR03017
- Wan, J., & Wilson, J. L. (1994b). Visualization of the role of the gas—water interface on the fate and transport of colloids in porous media. Water Resources Research, 30(1), 11–23. https://doi.org/10.1029/93WR02403
- Wang, J., Chen, Y., & Blau, W. J. (2008). Critical review: Nanomaterials in the environment: Behavior, fate, bioavailability, and effects.
- Wang, J., Chen, Y., & Blau, W. J. (2009). Carbon nanotubes and nanotube composites for nonlinear optical devices. *Journal of Materials Chemistry*, 19(40), 7425. https://doi.org/10.1039/b906294g
- Wang, M., Gao, B., & Tang, D. (2016). Review of key factors controlling engineered nanoparticle transport in porous media. *Journal of Hazard-ous Materials*, 318, 233–246. https://doi.org/10.1016/j.jhazmat.2016.06.065
- Wang, Y., & Hu, A. (2014). Carbon quantum dots: Synthesis, properties and applications. *Journal of Materials Chemistry C*, 2(34), 6921–6939. https://doi.org/10.1039/C4TC00988F
- Xu, S., Gao, B., & Saiers, J. E. (2006). Straining of colloidal particles in saturated porous media. Water Resources Research, 42, W12S16. https://doi.org/10.1029/2006WR004948
- Zevi, Y., Dathe, A., Gao, B., Richards, B. K., & Steenhuis, T. S. (2006). Quantifying colloid retention in partially saturated porous media. Water Resources Research, 42, W12S03. https://doi.org/10.1029/2006WR004929
- Zhang, M., Bradford, S. A., Šimůnek, J., Vereecken, H., & Klumpp, E. (2016). Do goethite surfaces really control the transport and retention of multi-walled carbon nanotubes in chemically heterogeneous porous media? *Environmental Science & Technology*, 50(23), 12713–12721. https://doi.org/10.1021/acs.est.6b03285
- Zhang, M., Bradford, S. A., Šimůnek, J., Vereecken, H., & Klumpp, E. (2019). Co-transport of multi-walled carbon nanotubes and sodium dodecylbenzenesulfonate in chemically heterogeneous porous media. *Environmental Pollution*, 247, 907–916. https://doi.org/10.1016/j. envnol.2019.01.106
- Zhao, Y. (2015). The use of nanoparticles to assess subsurface flow heterogeneity. Cornell University.

MAY ET AL. 12 of 12